

# Isospin and symmetry energy effects on nuclear fragment production in liquid-gas type phase transition region

N. Buyukcizmeci<sup>1</sup>, R. Ogul<sup>1,2</sup> and A.S. Botvina<sup>2,3</sup>

<sup>1</sup> Department of Physics, University of Selçuk, 42075 Konya, Turkey.

<sup>2</sup> Gesellschaft für Schwerionenforschung, D-64291 Darmstadt, Germany.

<sup>3</sup> Institute for Nuclear Research, Russian Academy of Science, RU-117312 Moscow, Russia.

Received: date / Revised version: date

**Abstract.** We have demonstrated that the isospin of nuclei influences the fragment production during the nuclear liquid-gas phase transition. Calculations for  $Au^{197}$ ,  $Sn^{124}$ ,  $La^{124}$  and  $Kr^{78}$  at various excitation energies were carried out on the basis of the statistical multifragmentation model (SMM). We analyzed the behavior of the critical exponent  $\tau$  with the excitation energy and its dependence on the critical temperature. Relative yields of fragments were classified with respect to the mass number of the fragments in the transition region. In this way, we have demonstrated that nuclear multifragmentation exhibits a 'bimodality' behavior. We have also shown that the symmetry energy has a small influence on fragment mass distribution, however, its effect is more pronounced in the isotope distributions of produced fragments.

**PACS.** 25.70.Pq Multifragment emission and correlations – 21.65.+f Nuclear matter – 24.60.-k Statistical theory and fluctuations

## 1 Introduction

One of the most interesting phenomena in heavy ion reactions is multifragmentation of nuclei, which is a very promising process to determine the properties of nuclear matter at subnuclear densities and high excitation energies. Experimental and theoretical analysis of this phenomenon is also very important for our understanding of astrophysical events, such as supernova explosions and formation of neutron stars [1,2]. The ground state properties of nuclear matter can usually be determined as a theoretical extrapolation, based on nuclear models designed to describe the structure of real nuclei. When nuclei are excited, these ground state properties show small changes without structural effects. At very high excitation energies ( $E^* > 2 - 3$  MeV/nucleon) the nuclei can slowly expand by remaining in a state of the thermodynamic equilibrium. During this expansion, they enter the region of subsaturation densities, where they become unstable to density fluctuations, and break up into the fragments (droplet formation). In this case, it is believed that a liquid-gas type phase transition is manifested. Even though there exist some theoretical and experimental evidences of this phase transition, so far some uncertainties remain in its nature [3,4,5,6,7,8,9,10,11]. Recently, the problem of isospin effects in multifragmentation gains a lot of interest in connection with the astrophysical applications. The main goal of this paper is to analyze these effects in the framework of a realistic model.

## 2 Statistical multifragmentation model

A model used for extracting the properties of nuclear matter, should be capable of reproducing the observed fragmentation properties. Statistical multifragmentation model (SMM) [12,13] has provided a good reproduction of experimental data, as shown by many experimental analyses [7,9,13,14,15,16,17]. Within the SMM we consider the whole ensemble of breakup channels consisting of hot fragments and nucleons in the freeze-out volume. In finite nuclear systems the SMM takes into account the conservation laws of energy  $E^*$ , momentum, angular momentum, mass number  $A_0$  and charge number  $Z_0$ . An advantage of SMM is that it considers all break-up channels including the compound nucleus and one can study the competition among them. In this respect, there is a natural connection between multifragmentation and traditional decay channels of nuclei as the evaporation and fission at low excitation energies. On the other hand the SMM can also address the thermodynamical limit, i.e. very large systems, that makes it suitable for astrophysical applications [2]. The probability of any breakup channel is assumed to be proportional to its statistical weight, and the channels are generated by the Monte Carlo method. The physical quantities such as average mass and charge fragment yields, temperature and its variance are calculated by running the summations over all members of the ensemble.

In this work we use the SMM version described fully in [13]. However, for this paper, it is important to explain how the hot primary fragments are treated. Light

fragments with mass number  $A \leq 4$  and charge number  $Z \leq 2$  are considered as stable particles (“nuclear gas”) with masses and spins taken from the nuclear tables. Only translational degrees of freedom of these particles contribute to the entropy of the system. Fragments with  $A > 4$  are treated as heated nuclear liquid drops, and their individual free energies  $F_{AZ}$  are parameterized as a sum of the bulk, surface, Coulomb and symmetry energy contributions

$$F_{AZ} = F_{AZ}^B + F_{AZ}^S + E_{AZ}^C + E_{A,Z}^{sym}. \quad (1)$$

The bulk contribution is given by  $F_{AZ}^B = (-W_0 - T^2/\epsilon_0)A$ , where  $T$  is the temperature, the parameter  $\epsilon_0$  is related to the level density, and  $W_0 = 16$  MeV is the binding energy of infinite nuclear matter. Contribution of the surface energy is  $F_{AZ}^S = B_0 A^{2/3} (\frac{T_c^2 - T^2}{T_c^2 + T^2})^{5/4}$ , where  $B_0 = 18$  MeV is the surface coefficient, and  $T_c = 18$  MeV is the critical temperature of the infinite nuclear matter. Coulomb energy contribution is  $E_{AZ}^C = cZ^2/A^{1/3}$ , where  $c$  is the Coulomb parameter obtained in the Wigner-Seitz approximation,  $c = (3/5)(e^2/r_0)(1 - (\rho/\rho_0)^{1/3})$ , with the charge unit  $e$ ,  $r_0 = 1.17$  fm, and  $\rho_0$  is the normal nuclear matter density  $\sim 0.15 fm^{-3}$ . And finally, the symmetry term is  $E_{A,Z}^{sym} = \gamma(A - 2Z)^2/A$ , where  $\gamma = 25$  MeV is the symmetry energy parameter. All the parameters given above are taken from the Bethe-Weizsäcker formula and correspond to the assumption of isolated fragments with normal density in the freeze-out configuration. This assumption has been found to be quite successful in many applications. However, for a more realistic treatment one should consider the expansion of the primary fragments in addition to their excitations. The residual interactions among them should be considered as well. These effects can be taken into account in the fragment free energies by changing the corresponding liquid-drop parameters.

Here, we have applied the SMM model to nuclear sources of different mass and isospin which can easily be used in modern experiments. The excitation energy range is of  $E^* = 2 - 20$  MeV/nucleon, and the freeze-out volume, where the intermediate mass fragments are located after expansion of the system, is  $V = 3V_0$  ( $V_0 = 4\pi A_0 r_0^3/3$  is the volume of a nucleus in its ground state). In other words, the fragment formation is described at a low density freeze-out ( $\rho \approx \rho_0/3$ ), where the nuclear liquid and gas phases coexist. The SMM phase diagram has already been under intensive investigations (see e.g. [18]) with the same parametrization of the surface tension of fragments versus the critical temperature  $T_c$  for the nuclear liquid-gas phase transition in infinite matter. Therefore, it is possible to extract  $T_c$  from the fragmentation data [19]. The symmetry energy contributes to the masses of fragments as well. Taking this contribution into account we shall investigate the influence of the symmetry energy coefficient  $\gamma$  on fragment production in the multifragmentation of finite nuclei. In this paper we concentrate mainly on properties of hot fragments. However, their secondary deexcitation is important for final description of the data, which was included in SMM long ago, and its effects were already discussed somewhere else ([13,19,20]). Here we

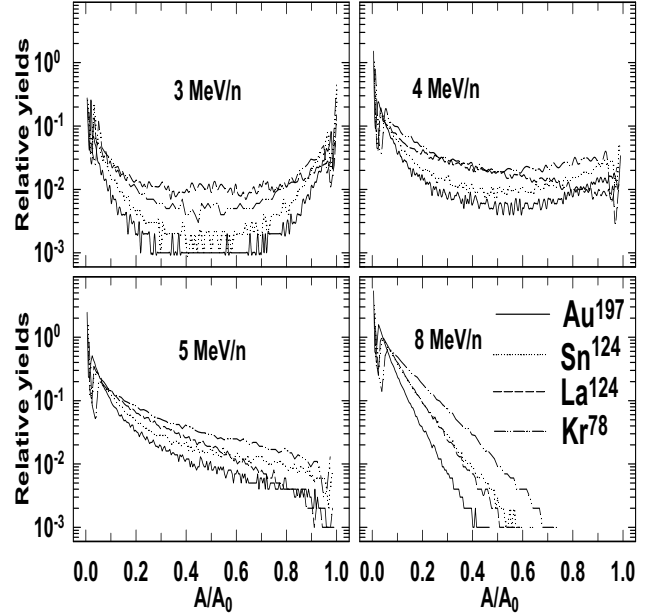


**Fig. 1.** Relative yield of hot primary fragments versus  $A/A_0$  for  $Au^{197}$ ,  $Sn^{124}$ ,  $La^{124}$  and  $Kr^{78}$  at different excitation energies 3, 4, 5 and 8 MeV/nucleon.

demonstrate how the secondary deexcitation code can be modernized so that the change in the symmetry energy of nuclei during the evaporation is taken into account.

### 3 Isospin dependence of fragment distributions

For our calculations, we consider  $Au^{197}$ ,  $Sn^{124}$ ,  $La^{124}$  and  $Kr^{78}$  nuclei to see how isospin affects the multifragmentation phenomena with their neutron-to-proton ratios ( $N/Z$ ), which read 1.49, 1.48, 1.18 and 1.17 respectively. The two sources  $Au^{197}$  and  $Sn^{124}$  have nearly the same  $N/Z$  ratios 1.49 and 1.48, respectively, but different mass numbers, whereas  $Sn^{124}$  and  $La^{124}$  have the same mass numbers, but very different  $N/Z$  ratios 1.48 and 1.18, respectively. To see the effect of the size of the nucleus in our study, we have also included  $Kr^{78}$ , which has the lowest mass number among the considered nuclei here, but its  $N/Z$  ratio 1.17 is very close to that of  $La^{124}$ . Relative yield of hot fragments produced after the break-up of  $Au^{197}$ ,  $Sn^{124}$ ,  $La^{124}$  and  $Kr^{78}$  nuclei as a function of  $A/A_0$  is given in Fig. 1 for  $E^* = 3, 4, 5$  and 8 MeV/nucleon. As was shown in previous analysis of experimental data (see e.g. [7,9,13,15]) these results are fully consistent with experimental observations. The effect of isospin of different sources in liquid-gas phase transition region can be clearly seen for different excitation energies. The mass distribution of fragments produced in the disintegration of various nuclei evolves with the excitation energy. As can be seen in Fig. 1, for  $Au^{197}$  and  $Sn^{124}$  multifragmentation onset is about 5 MeV/nucleon and for  $La^{124}$  and  $Kr^{78}$  it is about

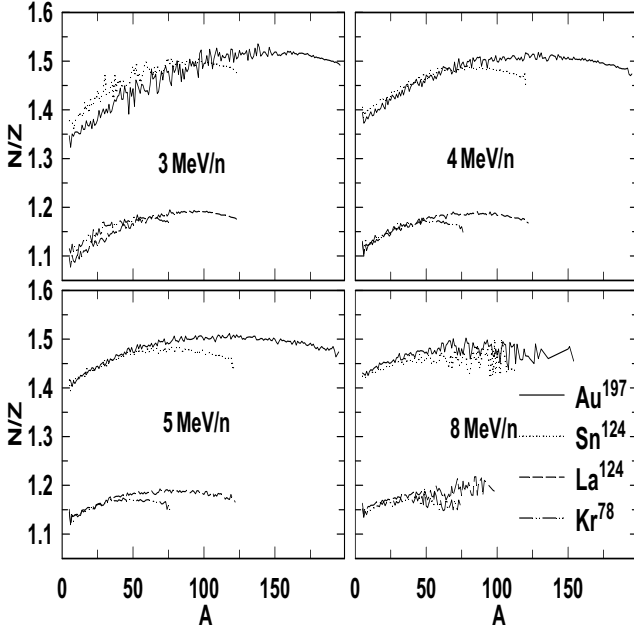


**Fig. 2.**  $N/Z$  ratio of hot primary fragments versus  $A$  for  $Au^{197}$ ,  $Sn^{124}$ ,  $La^{124}$  and  $Kr^{78}$  at different excitation energies 3, 4, 5 and 8 MeV/nucleon.

4 MeV/nucleon at standard SMM parameters so that U-shape mass distributions disappear at these energies. We can also describe this evolution with the temperature (see the caloric curves below). At low temperatures ( $T \leq 5$  MeV), there is a U-shape distribution corresponding to partitions with few small fragments and one big residual fragment. At high temperatures ( $T \geq 6$  MeV), the big fragments disappear and an exponential-like fall-off is observed. In the transition region ( $T \simeq 5 - 6$  MeV), however, one observes a transition between these two regimes, which is rather smooth because of finiteness of the systems.

In Fig. 2 we demonstrate  $N/Z$  ratios of the hot fragments produced in the freeze-out volume of the same systems. One can see that neutron content of hot fragments is only slightly smaller than that of the whole system since the most of the neutrons are still contained in fragments. It is also seen that the neutron richness of fragments is increasing with their mass number [21]. This is a general behavior for nuclear systems in equilibrium, where binding energy is influenced by interplay of the Coulomb and the symmetry energy. For some systems one can observe specific isotopic effects such as the increasing of the neutron richness of intermediate mass fragments (with  $Z=3-20$ ) with the excitation energy (compare the results for 3 and 8 MeV/nucleon). This is because after removing heavy fragments by increasing excitation energy, their neutrons are accumulated into the smaller fragments [21].

Usually a power-law fitting is performed with,  $Y(A) \propto A^{-\tau}$  and  $Y(Z) \propto Z^{-\tau_Z}$ , where  $Y(A)$  and  $Y(Z)$  denote the multifragmentation mass and charge yield as a function of fragment mass number  $A$  and charge number  $Z$ ,

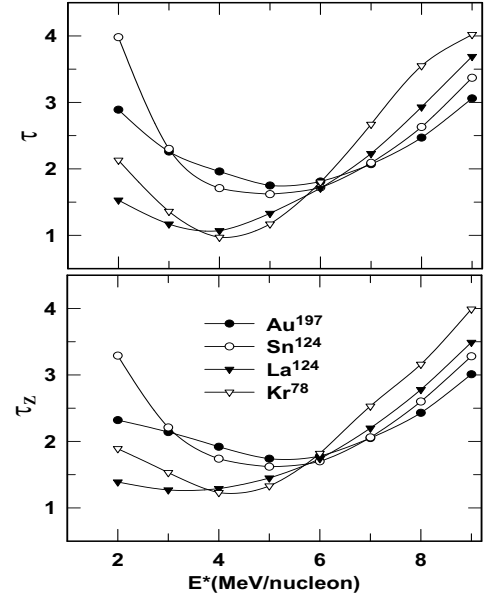


**Fig. 3.** The values of critical exponents  $\tau$  (top panel) and  $\tau_Z$  (bottom panel), as a function of excitation energy  $E^*$  for  $Au^{197}$ ,  $Sn^{124}$ ,  $La^{124}$  and  $Kr^{78}$ .

respectively. The parameters  $\tau$  (for mass distribution) and  $\tau_Z$  (for charge distribution) can be considered in thermodynamical limit as critical exponents [16,22]. In calculations, we consider the fragments in the range  $6 \leq A \leq 40$  for mass and  $3 \leq Z \leq 18$  for charge number. The lighter fragments are considered as a nuclear gas. The obtained values of  $\tau$  and  $\tau_Z$  at  $T_c = 18$  MeV as a function of  $E^*$  are given in Fig. 3 for cold fragmentation (with secondary de-excitation). There is a minimum at about  $E^* = 5.3, 5.2, 4$  and  $4.2$  MeV/nucleon for  $Au^{197}$ ,  $Sn^{124}$ ,  $La^{124}$  and  $Kr^{78}$ , respectively. The results for  $Au^{197}$  and  $Sn^{124}$  are very similar to each other and significantly different from those obtained for  $La^{124}$  and  $Kr^{78}$ . This means that intermediate mass fragment (IMF) distributions approximately scale with the size of the sources, and they depend on the neutron-to-proton ratios of the sources. This is because the symmetry energy still dominates over the Coulomb interaction energy for these intermediate-size sources. One may also see from these results that the lower  $N/Z$  ratio leads to smaller  $\tau$  and  $\tau_Z$  parameters with the flatter fragment distribution. A large  $N/Z$  ratio of the source favors the production of big clusters since they have a large isospin. This is the reason for domination of partitions consisting of small IMFs with a big cluster in the transition region (U-shape distribution). It is also seen from the bottom of Fig. 3 that the values of  $\tau_Z$  are very close to the values of  $\tau$  since the neutron-to-proton ratio of produced IMFs exhibits a small change within their narrow charge range (see also [15,21]).

For completeness, we have calculated the average IMF multiplicity and its variance for the excitation energy range of 2 – 20 MeV/nucleon for all nuclei. To avoid the effect of the source size and leave only the isospin effect, IMF mul-

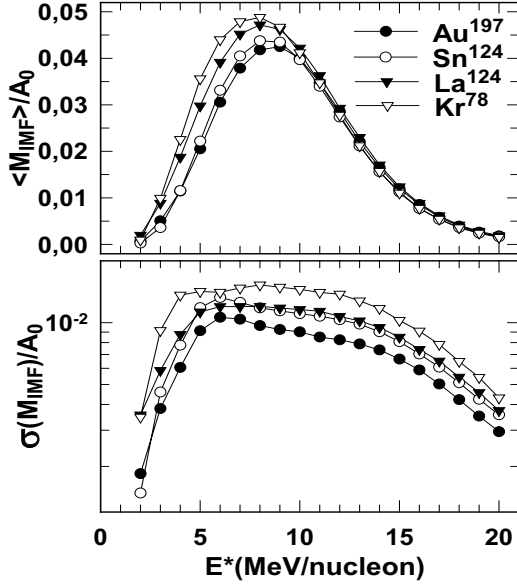


**Fig. 4.** The average IMF multiplicity (top panel) and its variance (bottom panel) per nucleon versus  $E^*$  for various nuclei.

tiplicity is divided by  $A_0$ . In Fig. 4, we present the scaled average IMF multiplicity and its variance versus  $E^*$ . In this figure, one may clearly see an effect of the isospin and the source size on fragment multiplicities.

#### 4 Largest fragments in fragment partitions

In multifragmentation, the mass number of the largest fragment  $A_{max}$  may be used as an "order parameter" since it is directly related to the number of fragments produced during disintegration. We have analyzed its behavior with respect to the excitation energies. In order to remove the effect of source size and leave only an isospin effect, we have scaled it with the mass number of the source  $A_0$ . We have plotted  $A_{max}/A_0$  as a function of excitation energy in Fig. 5 (top panel). The values of these quantities decrease first rapidly with  $E^*$ , and then, beyond some value ( $E^* \sim 10$  MeV/nucleon), decrease rather slowly. This suggests that the vaporization process becomes dominant around this point (see also an analysis in Ref. [16]). Another striking result of this behavior is that all curves almost coincide in the transition region as displayed on the top panel in Fig. 5 (i.e. a universality of the behavior of  $A_{max}$ ). We have also calculated the average  $A_{max}$  variances in the multifragmentation stage for all nuclei at the same excitation energy range. The average variance of  $A_{max}/A_0$  values are presented in the bottom panel of Fig. 5. We observe from this figure that the maximum variance values for all sources are seen at an excitation energy of 4 – 5 MeV/nucleon, which is exactly corresponding to the region of the transition from compound-like channels to the full multifragmentation. In the following we clarify why this kind of behavior takes place.

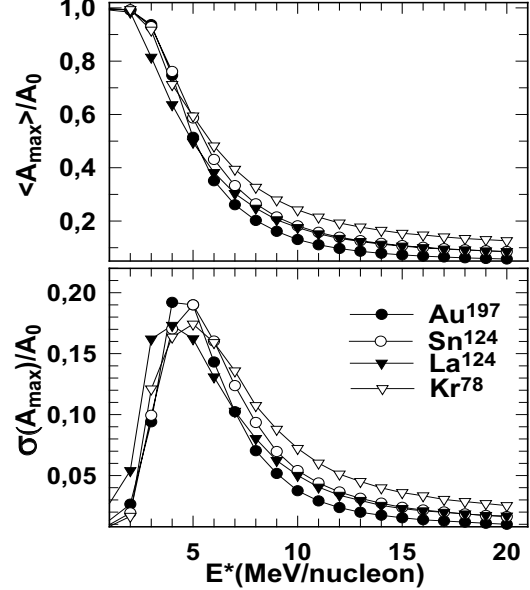


**Fig. 5.**  $\langle A_{max} \rangle$  and its variance  $\sigma(A_{max})$  divided by  $A_0$  versus  $E^*$  for  $Au^{197}$ ,  $Sn^{124}$ ,  $La^{124}$  and  $Kr^{78}$ .

#### 5 Temperature and bimodality

Temperature of fragments is an important ingredient for any description of nuclear multifragmentation. Besides statistical approaches, a temperature can even be introduced in dynamical (coalescence-like) processes of fragment production [23]. In SMM, the temperature of fragments  $T_f$  in separate partitions is defined from their energy balance according to the canonical prescription:

$$m_0 + E^* = 1.5(n-1)T_f + \sum_i (m_i + E_i^*(T_f)) + E_{coul}, \quad (2)$$

where  $n$  is multiplicity of hot fragments and 'gas' particles,  $m_0$  and  $m_i$  are ground masses of initial nucleus and the fragments,  $E_i^*$  are internal excitation energies of fragments, and  $E_{coul}$  is their Coulomb interaction energy. Masses and internal excitations are found according to their free energies (see eq. (1) and Ref. [13]). The term with  $(n-1)$  takes into account the center of mass constraint, which is important for finite systems [24]. In this approach we allow for temperature to fluctuate from partition to partition, and we define the temperature of the system as the average one for the generated partitions. The methods involving fluctuations of temperature have been used in thermodynamics since long ago [25]. Our definition of temperature has another advantage: It is fully consistent with the temperature commonly used in nuclear physics for isolated nuclei, that makes a natural connection with the physics of compound nucleus.

Figs. 6a and 6b show the results of the average temperature and its variance with respect to the excitation energy  $E^*$  for all nuclei under consideration. While one may see a plateau in the excitation energy range 3 – 7 MeV/nucleon in the upper panel of this figure, the variance of temperature exhibits a maximum value at about

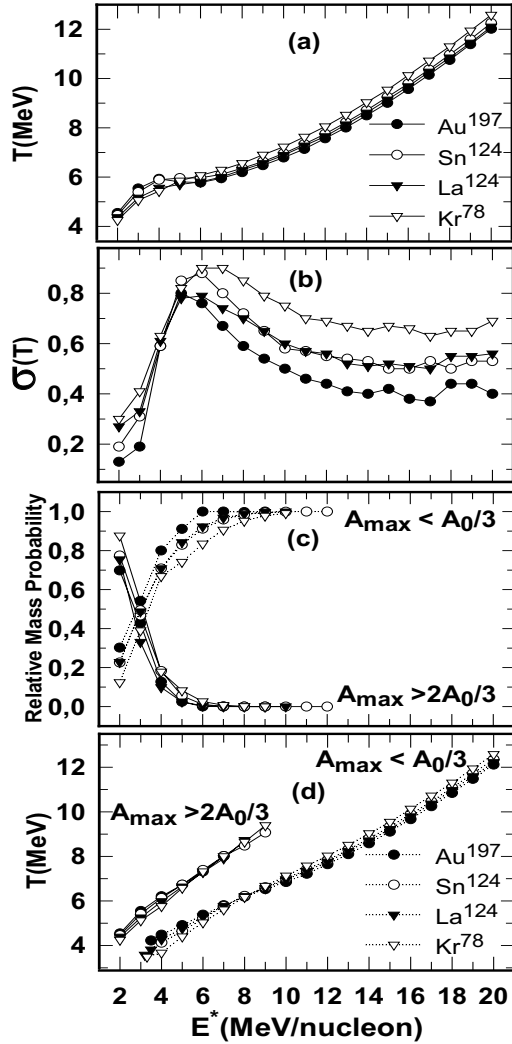


**Fig. 6.** (a) Temperature, (b) its variance value, (c) probabilities of events with  $A_{max} > 2A_0/3$  and  $A_{max} < A_0/3$  and (d) average temperatures  $T$  versus  $E^*$  for  $Au^{197}$ ,  $Sn^{124}$ ,  $La^{124}$  and  $Kr^{78}$ . The full and dotted lines in Fig.6c and 6d represent the events with  $A_{max} > 2A_0/3$  and  $A_{max} < A_0/3$ , respectively.

5 – 6 MeV for standard SMM parameters, in agreement with the maximum fluctuations of  $A_{max}$ . The plateau-like caloric curve was reported long ago (e.g. [12,13]). It was confirmed by experimental results [26], and by rather sophisticated calculations of Fermionic Molecular Dynamics [27] and Antisymmetrized Molecular Dynamics [28]. The reason for large fluctuations of the temperature and  $A_{max}$ , can be clear from Figs. 6c and 6d. In these figures we show relative mass probability and temperature values for two groups of fragment partitions, which are defined as  $A_{max} > 2A_0/3$  (associated with compound-like channels) and  $A_{max} < A_0/3$  (full multifragmentation). As can be seen in Fig. 6c, the probability of observing the first group events  $A_{max} > 2A_0/3$  decreases rapidly in the excitation energy range 2 – 6 MeV/nucleon, and this probability for the second group  $A_{max} < A_0/3$  increases within the same

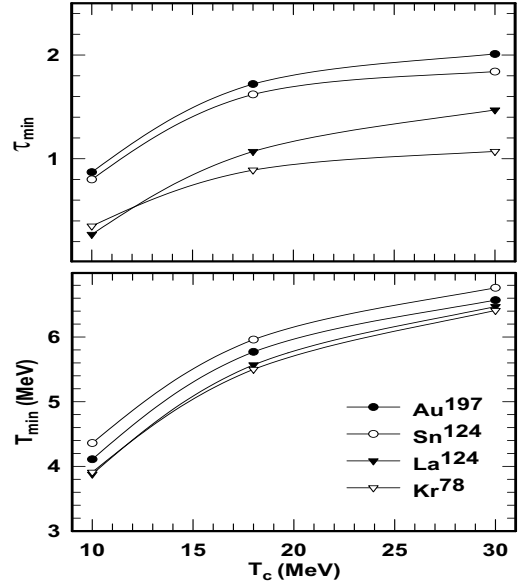


**Fig. 7.** The values of  $\tau_{min}$  and  $T_{min}$  as a function of the critical temperature  $T_c$  for various nuclei.

energy range. However, temperatures of these groups of fragments are essentially different, since the binding energy effect is different, and a disintegration into a large number of fragments takes more energy. The transition to the energy consuming group  $A_{max} < A_0/3$  occurs because of the phase space domination, despite of a smaller temperature of this group. We will call it 'bimodality' from now on (see also discussion for other models in [29]). It is an intrinsic feature of the phase space population in the SMM, however, it was only recently realized that it can be manifested in different branches of the caloric curve and in momenta of fragment distributions (see Ref. [7]). The bimodality provides an explanation why the caloric curve may have a plateau-like (or even a 'back-bending') behavior and large fluctuations in the transition region.

## 6 Influence of the critical temperature

We have analyzed how the critical exponent  $\tau$  depends on  $T_c$ , similar to Ref. [19], and on isospin of the sources. During multifragmentation nuclei demonstrate critical behavior at considerably lower temperatures ( $T^* \approx 5 - 6$  MeV) than the critical temperature of nuclear matter  $T_c$  (see also [7,9,16]), because of Coulomb and finite size effects. As was shown in many papers (see e.g. [16] and references in) the critical behavior can manifest as scaling of some observables around the critical point  $T^*$ . In the present work we are interested in information about the critical temperature  $T_c$ , which is high enough to be extracted through the scaling in finite nuclei. However, this information can be obtained by looking at other features of fragment distributions, since the critical temperature influences the surface tension of fragments. We have extracted the minimum values of  $\tau$  versus  $T_c$  and the corresponding temperatures of

the systems, as shown in Fig. 7. The similar analysis of experimental data was carried out by Karnaukhov et al. [17] for residues produced after intranuclear cascade in Au target. One can see from Fig. 7 that both the  $\tau_{min}$  and  $T_{min}$  the temperature corresponding to this minimum, increase with  $T_c$ . However, nuclei with lower isospin such as  $La^{124}$  and  $Kr^{78}$  exhibit much lower  $\tau_{min}$  values. It is because of the proton-rich nuclei are less stable, and they disappear rapidly with the excitation energy, this corresponds to a less pronounced U-shape mass distribution. This effect may be important for explanation of some data, since sources with different isospin may manifest different  $\tau_{min}$ . The decreasing  $T_{min}$  for lower  $T_c$  is explained by a very fast decreasing of the surface tension with temperature in this case. Nevertheless, all parameters increase with  $T_c$ , and tend to saturate at  $T_c \rightarrow \infty$ , corresponding to the case of the temperature-independent surface. In this case only the translational and bulk entropies of fragments, but not the surface entropy, influence the probability of fragment formation.

## 7 Influence of the symmetry energy

Now let us turn to the analysis of the symmetry energy of fragments, and its influence on fragment partitions. As we discussed, the symmetry energy for fragments is defined in SMM as  $E^{sym} = \gamma(A - 2Z)^2/A$ , where  $\gamma$  is a phenomenological coefficient. As an initial approximation for the SMM calculations we assume  $\gamma=25$  MeV, corresponding to the mass formula of cold nuclei. We have also performed the calculations for  $\gamma=8$  MeV for  $Sn^{124}$  and  $La^{124}$  sources. In Fig. 8 we demonstrate the caloric curve, the mean maximum mass of fragments in partitions, and  $\tau$  parameters for different assumptions on the symmetry energy. The results for  $\gamma=8$  MeV are only slightly different from those obtained for the standard SMM assumption  $\gamma=25$  MeV. From this figure, one can see a small decrease of temperature caused by the involvement of the fragments with unusual neutron and proton numbers into the dominating partitions. Therefore, the average characteristics of produced hot fragments are not very sensitive to the symmetry energy, and special efforts should be taken in order to single out this effect.

The main effect of the symmetry energy is manifested in charge and mass variances of the hot fragments. In Fig. 9 we have shown the relative mass distributions of primary hot (top panels) and final cold fragments (after secondary deexcitation, middle and bottom panels) with  $Z = 5$  and 10 at an excitation energy of 5 MeV/n for  $\gamma = 25$  and 8 MeV. The distribution of primary hot fragments becomes rather broad for  $\gamma = 8$  MeV and its maximum lies on the neutron-rich side.

## 8 Evaporation of hot fragments with isospin effects

The primary fragments are supposed to decay by secondary evaporation of light particles, or by the Fermi-

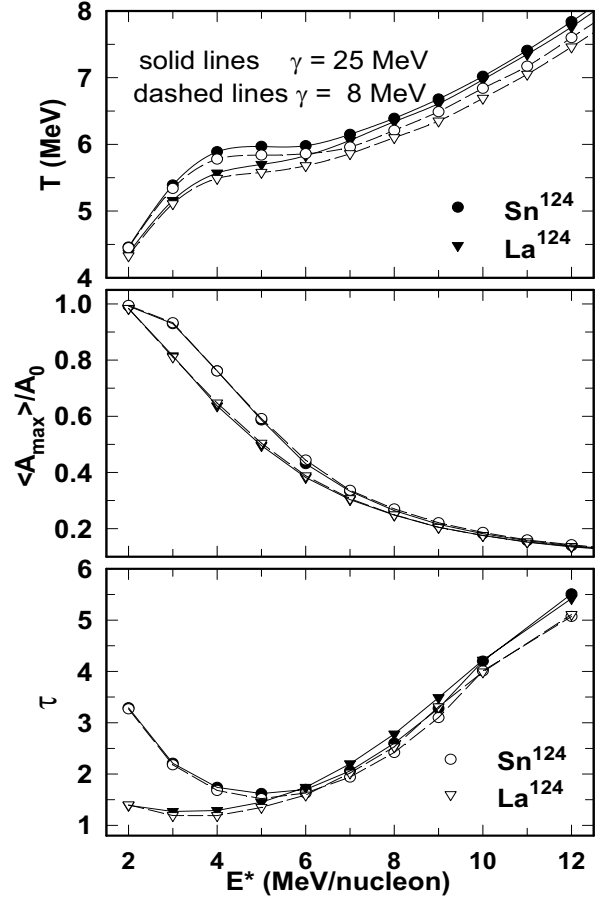
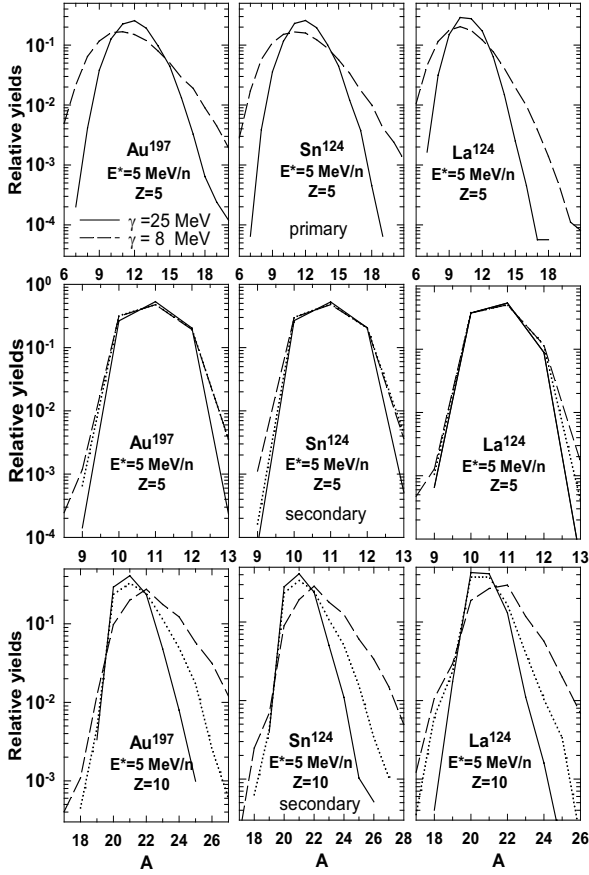


Fig. 8. Variation of the caloric curves (top panel),  $A_{max}/A_0$  (middle) and  $\tau$  (bottom) of the nuclei  $Sn^{124}$  and  $La^{124}$  with symmetry energy versus excitation energy.

break-up [20,13]. However, these codes use standard mass formulae obtained from fitting masses of cold isolated nuclei. If hot fragments in the freeze-out have smaller values of  $\gamma$ , their masses in the beginning of the secondary deexcitation will be different, and this effect should be taken into account in the evaporation process. Sequential evaporation is considered only for large nuclei ( $A > 16$ ) evaporating lightest particles ( $n, p, d, t, {}^3He, \alpha$ ). We believe that we can estimate the effect of the symmetry energy evolution during the sequential evaporation by including the following prescription. There are two different regimes in this process. First, in the case when the internal excitation energy of this nucleus is large enough ( $E^*/A > 1$  MeV), we take for hot fragments the standard liquid drop masses  $m_{ld}$  adopted in the SMM, as follows

$$m_{AZ} = m_{ld}(\gamma) = m_n N + m_p Z - AW_0 + \gamma \frac{(A-2Z)^2}{A} + B_0 A^{2/3} + \frac{3e^2 Z^2}{5r_0 A^{1/3}}, \quad (3)$$

where  $m_n$  and  $m_p$  are masses of free neutron and proton. In the second regime corresponding to the lower excitation energies, we adopt a smooth transition to standard experimental masses with shell effects ( $m_{st}$ , taken from



**Fig. 9.** Isotopic distribution of primary and secondary fragments for  $Z = 5$  and  $Z = 10$  versus mass number  $A$  at an excitation energy of 5 MeV/nucleon for  $Au^{197}$ ,  $Sn^{124}$  and  $La^{124}$ . At  $\gamma=8$  MeV the results after standard secondary decay are shown with dotted lines, and dashed lines denote the results of new evaporation depending on the symmetry energy (see the text).

nuclear tables) with the following linear dependence,

$$m_{AZ} = m_{id}(\gamma) \cdot x + m_{st} \cdot (1 - x), \quad (4)$$

where  $x = \beta E^*/A$  ( $\beta = 1\text{MeV}^{-1}$ ) and  $x \leq 1$ . The excitation energy  $E^*$  is always determined from the energy balance taking into account the mass  $m_{AZ}$  at the given excitation. This mass correction was included in a new evaporation code developed on the basis of the old model [20], taking into account the conservation of energy, momentum, mass and charge number. We have checked that the new evaporation at  $\gamma=25$  MeV leads to the results very close to those of the standard evaporation.

Generally, the secondary deexcitation pushes the isotopes towards the value of stability, however, the final distributions depend on the initial distributions for hot fragments. One can see that the results can also depend on whether the symmetry energy evolves during the evaporation or not. In Fig. 9 we demonstrate the results of two kind of calculations. First one is carried out according

to the standard code [20] and the second one is with the above described version taking into account the symmetry energy (mass) evolution during evaporation. The standard deexcitation leads to narrowing the distributions and to concentration of isotopes closer to the  $\beta$ -stability line by making the final distributions of the case of  $\gamma=8$  MeV similar to the case of  $\gamma=25$  MeV. However, a sensitivity to the initial values of  $\gamma$  remains, as one can see from distributions of cold fragments with  $Z=5$  and 10. This difference in distributions is much more pronounced if we use the new evaporation. The final isotope distributions are considerably wider, and they are shifted to the neutron rich side, i.e. the produced fragments are neutron rich. This effect has a simple explanation: By using the experimental masses at all steps of evaporation we suppress emission of charged particles by both the binding energy and the Coulomb barrier. Whereas, in the case of small  $\gamma$  in the beginning of evaporation, the binding energy essentially favors an emission of charged particles. When the nucleus is cooled sufficiently down to restore the normal symmetry energy, the remaining excitation is rather low ( $E^*/A < 1$  MeV) for the nucleus to evaporate many neutrons.

The difference between the two kind of evaporation calculations gives us a measure of uncertainty expected presently in the model. This uncertainty can be diminished by comparison with experiments. It is encouraging, however, that all final isotope distributions have some dependence on the  $\gamma$  parameter. This sensitivity gives us a chance to estimate the symmetry energy by looking at isotope characteristics. As was shown earlier the actual  $\gamma$  parameter of the symmetry energy can be determined via an isoscaling analysis [30]. An analysis of  $N/Z$  ratio of produced fragments can also be used for this purpose. Recently one may see some experimental evidences for essential decreasing of the symmetry energy of fragments with temperature in multifragmentation [31,32]. The consequences of this decreasing are very important for astrophysical processes [2].

## 9 Conclusions

In summary, we have shown the effects of isospin, critical temperature and symmetry energy on the fragment distribution in multifragmentation. For this purpose we have analyzed different nuclei with various neutron-to-proton ratio on the basis of SMM. The critical temperature of nuclear matter influences the fragment production in multifragmentation of nuclei through the surface energy, while the symmetry energy determines directly the neutron richness of the produced fragments. Effects of the critical temperature can be observed in the power law fitting parametrization of the fragment yields by finding  $\tau$  parameter. We have also shown the effect of the isospin and neutron excess of sources on the fragment distributions and on the  $\tau$  parametrization. By selecting partitions according to the maximum fragment charge we have demonstrated a bimodality as an essential feature of the phase transition in finite nuclear systems. This feature may allow for identification of this phase transition

with the first order one. It has been found out that the symmetry energy of the hot fragments produced in the statistical freeze-out is very important for isotope distributions, but its influence is not very large on the mean fragment mass distributions after multifragmentation. We have shown that the symmetry energy effect on isotope distributions can survive after secondary deexcitation. An extraction of this symmetry energy from the data is important for nuclear astrophysical studies.

N.B. and R.O. thank Selcuk University-Scientific Research Projects (BAP) for a partial financial support under grant-SU-2003/033. The authors gratefully acknowledge the enlightening discussions with W. Trautmann, J. Lukasik, I.N. Mishustin, V.A. Karnaukhov and U. Atav. We also thank GSI for hospitality, where part of this work was carried out. R. Ogul gratefully acknowledges the financial support by DAAD as well.

## References

1. H.A. Bethe, Rev. Mod. Phys. **62**, 801 (1990).
2. A.S. Botvina and I.N. Mishustin, Phys. Lett. B **584**, 233 (2004).
3. A.L. Goodman, J.I. Kapusta and A.Z. Mekjian, Phys. Rev. C **30**, 851 (1984).
4. C.J. Pethick, D.G. Ravenhall, Nucl. Phys. **A471**, 19c (1987).
5. R. Ogul, Int. J. Mod. Phys. E, **7(3)**, 419 (1998).
6. A.B. Larionov, I.N. Mishustin, Sov. J. Nucl. Phys. **57**, 636 (1994).
7. M. D'Agostino *et al.*, Nucl. Phys. A **650**, 329 (1999).
8. W. Bauer and A. Botvina, Phys. Rev. **C52**, R1760 (1995).
9. J.A. Hauger *et al.*, Phys. Rev. **C62**, 024616 (2000).
10. J. Schmelzer *et al.*, Phys. Rev. C **55**, 1917 (1997).
11. M. Mahi *et al.*, Phys. Rev. Lett. **60**, 1936 (1988).
12. A.S. Botvina, A.S. Iljinov, I.N. Mishustin, Sov. J. Nucl. Phys. **42**, 712 (1985).
13. J.P. Bondorf, A.S. Botvina, A.S. Iljinov, I.N. Mishustin, and K. Sneppen, Phys. Rep. **257**, 133 (1995).
14. M. D'Agostino *et al.*, Phys. Lett **B371**, 175 (1996).
15. A.S. Botvina *et al.*, Nucl. Phys. **A584**, 737 (1995).
16. B.K. Srivastava *et al.*, Phys. Rev. C **65**, 054617 (2002).
17. V.A. Karnaukhov *et al.*, Phys. Rev. C **67**, R011601 (2003).
18. K.A. Bugaev *et al.*, Phys. Rev. **C62**, 044320 (2000).
19. R. Ogul and A.S. Botvina, Phys. Rev. C **66**, R051601 (2002).
20. A.S. Botvina *et al.*, Nucl. Phys. **A475**, 663 (1987).
21. A.S. Botvina and I.N. Mishustin, Phys. Rev. C **63**, 061601 (2001).
22. P.T. Reuter, K.A. Bugaev, Phys. Lett. B **517**, 233 (2001).
23. W. Neubert and A.S. Botvina, Eur. Phys. J. A **17**, 559 (2003).
24. A.S. Botvina and I.N. Mishustin, Phys. Rev. Lett. **90**, 179201 (2003).
25. L.D. Landau and E.M. Lifshitz, Statistical Physics, Part 1 (3rd ed. Pergamon, New York, 1980) p.340.
26. W. Trautmann, Nucl. Phys. **A685**, 233 (2001).
27. J. Schnack, H. Feldmeier, Phys. Lett. B **409**, 6 (1997).
28. Y. Sugawa and H. Horiuchi, Phys. Rev. C **60**, 064607 (1999).
29. Ph. Chomaz *et al.*, Phys. Rev. E **64**, 046114 (2001).
30. A.S. Botvina, O.V. Lozhkin, W. Trautmann, Phys. Rev. C **65**, 044610 (2002).
31. A. Le Fevre *et al.*, Phys. Rev. Lett. **94**, 162701 (2005).
32. D.V. Shetty *et al.*, Phys. Rev. C **71**, 024602 (2005).